Dynamic regulation on energy landscape evolution of single-molecule protein by conformational fluctuation

Chien Y. Lin and Jung Y. Huang*
Department of Photonics and Institute of Electro-Optical Engineering, Chiao Tung University, Hsinchu 300, Taiwan, Republic of China

Leu-Wei Lo
Division of Medical Engineering Research, National Health Research Institutes, Zhunan, Miaoli 350, Taiwan, Republic of China

(Received 4 June 2012; published 31 August 2012)

We formalize a theory to help explore the effect of conformational fluctuation on the energy landscape evolution of single-molecule protein. Using this formalization, we investigate the photon emission from single photoactivated fluorescent protein. A bimodal regulation on the energy landscape evolution was discovered, and its origin was attributed to slow conformational fluctuations of the protein matrix.

DOI: 10.1103/PhysRevE.86.021925 PACS number(s): 87.10.Mn, 82.37.−j

I. INTRODUCTION

Many important molecular processes in biology, including protein folding and enzymatic reactions [1–6], rely critically on energy landscape evolution. The transitions between two distinct basins on the energy landscape often involve several intermediate steps [7–9]. Experimental studies have shown that enzymatic reactions follow closely the conformational changes of proteins [1–3]. It is interesting to note that some proteins even employ conformational fluctuations to improve chemical reactivity [10]. Bimodal regulations resulting from conformational fluctuations can be used to refine the selection among several competitive processes [11–14]. These observations raise an important question: How does an enzyme utilize its conformational fluctuation to dynamically regulate catalytic activity?

The energy landscape dynamics of an enzyme can be described by projecting the dynamics onto rate-limiting transitions [15–18]. This approach, however, will sometimes miss rare intermediate states that serve as the key steps on the way to the native state [19–22]. A quantitative description of the dynamics on a millisecond time scale is crucial for an understanding of the enzyme's catalytic mechanism. Unfortunately, proteins do not move synchronously, which results in averaging away conformational dynamics in ensemble measurements. Observing a single molecule in action can remove the ensemble average, thus allowing the exploration of hidden structural heterogeneity [4–6].

A detailed microscopic understanding of a single-molecule system is often precluded by a complex environment and thermal fluctuations. Therefore, it is difficult to fully interpret the data from single-molecule optical measurements. In this paper, we develop a formalization of single-molecule measurement that captures both the photon statistics and the complex energy landscape dynamics of an open quantum system. We reduced the problem down to a series of manageable tasks. This approach is particularly attractive in the study of proteins and enzymes in which an active site, which demands an accurate description of the physics, is embedded into another region, where a stochastic description is needed. To test the applicability and efficacy of our formalization, the photon emission dynamics of a single KFP1 photoactivated fluorescent protein [23–26] was analyzed.

II. THEORY

A. Energy landscape evolution of single-molecule protein

Figure 1(a) is a schematic diagram of a protein with an active center embedded in a complex environment. Apparently, the dynamics of an active center interacting with a complex environment cannot be described as a Markovian process [27]. However, a general treatment of the full non-Markovian action of the environment is not feasible. Therefore, we split the complex environment into a direct sum of subreservoirs by using the generalized Born-Markov approximation as proposed by Budini [28]. Linear combinations of the dissipative effects induced by each subreservoir were used to simulate the non-Markovian behaviors of the active center.

The dynamic evolutions of an active center in a protein are captured by the Liouville equation [29,30], $\partial_t G(t,s) = \mathcal{L}_{H_i} G(t,s)$, with a Liouville operator $\mathcal{L}_{H_i}[\bullet] = \frac{-i}{\hbar}[H_i(t),\bullet]$ defined by Hamiltonian H_i of the active center. In an open system, the active center is constantly perturbed by its environment. To further eliminate the internal complexity, we separated the impacts from the environment on the active center into two categories: the slow modulations that allow the active center to respond adiabatically, and the fast fluctuations with a speed higher than the dynamics of the active center. The response of the active center to the slow modulations was described by a series of stochastic matrix $\mathbb{M}$ to model the transitions between two local basins on the energy landscape. The generating function of the perturbed active center $\mathcal{G}(t,s) = G(t,s)e^{\int_0^t d\tau \mathbb{M}(\tau)} = \sum_{n=0}^{\infty} s^n \rho^{(n)}(t)$ satisfies $\partial_t \mathcal{G}(t,s) = (\mathcal{L}_{H_i} + \mathbb{M})\mathcal{G}(t,s)$. We described the response of the active center to the fast fluctuating environment with a memory kernel $K(t)$ [29]. The resulting density matrix evolution of the open system follows a Lindblad-like equation with an effective Hamiltonian $H_{\text{eff}}(t)$ comprising a stochastic Hamiltonian $H_p(t)$ from the environment and $H_i(t)$ from the active center [28],

$$\partial_t \mathcal{G}(t,s) = (\mathcal{L}_{H_i} + \mathbb{M})\mathcal{G}(t,s) + \int_0^t d\tau\, K(t-\tau)\mathcal{J}_D \mathcal{G}(\tau,s) = (\mathcal{L}_{H_i} + \mathcal{L}_{H_p})\mathcal{G}(t,s) = \mathcal{L}_{H_{\text{eff}}}\mathcal{G}(t,s). \quad (1)$$

*jyhuang@faculty.nctu.edu.tw

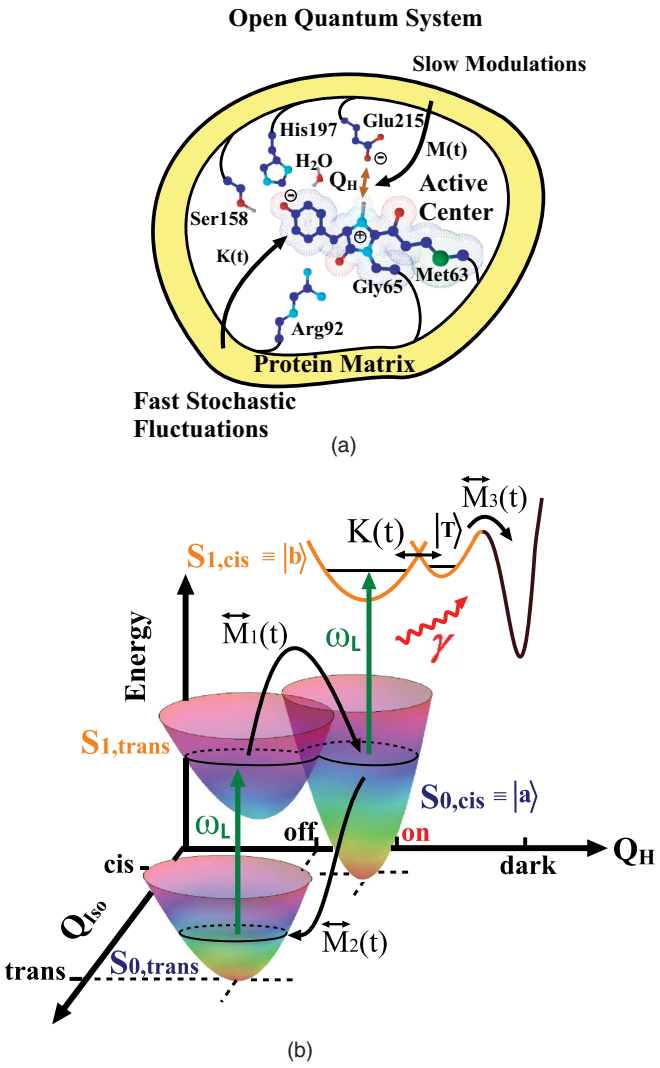

FIG. 1. (Color online) (a) Schematic of an open system of KFP1. (b) Model of the electronic structure of KFP1. The transition $\overleftrightarrow{M}_1$ begins after a green photon is absorbed to reach the excited state $S_{1,\mathrm{trans}}$ of KFP1. After overcoming the energy barrier at $S_{1,\mathrm{trans}}/S_{0,\mathrm{cis}}$, the chromophore becomes a *cis* configuration and is fluorescent. $\overleftrightarrow{M}_2$ is a thermally driven transition from the *cis* to the *trans* configuration. The irreversible photobleaching of the chromophore to the dark state is described by $\overleftrightarrow{M}_3$.

Here $\mathcal{L}_{H_p}[\bullet] = \mathbb{M}[\bullet] + \int_0^t d\tau K(t-\tau)\mathcal{J}_D[\bullet]$ is the superoperator describing the environmental impacts on the active center and $\mathcal{J}_D[\bullet] = -\frac{1}{2}\{\hat{\sigma}^\dagger\hat{\sigma},\bullet\}_+ + s\hat{\sigma}\bullet\hat{\sigma}^\dagger$ is the Lindblad superoperator, in terms of the Pauli matrices $\hat{\sigma}$ and the adjoint matrices $\hat{\sigma}^\dagger$, which links the dynamics of the active center and the environment.

We applied the formalism to a real biomolecular system KFP1. KFP1 is a photoactivated fluorescent protein, which is photoswitchable between a fluorescent on- and off-state along the reactive coordinate Q_{iso} with the chromophores in a *cis*- and *trans*-configuration, respectively. A hydrogen bonding (Q_H) formed between Glu215 and the N-H proton of the chromophore [see Fig. 1(a)] plays an important role in regulating the photon-emitting process of the chromophore [26]. The small mass of the hydrogen atom means that the hydrogen bond is inherently quantum mechanical in nature [31], and could serve as a sensitive structural indicator of the enzyme active site.

We split the open system of KFP1 into three components: a reservoir, a fluorescent quantum system, and a triplet state $|T\rangle$ [28], as illustrated in Fig. 1(b). The optically excited active center was modeled as a two-level quantum system with Hamiltonian $H_i(t) = \frac{1}{2}\hbar\omega_0(t)\hat{\sigma}_z + \hbar\Omega\cos(\omega_L t)\hat{\sigma}_x$. The energy difference between the excited state $|b\rangle$ and the ground state $|a\rangle$ of the *cis*-chromophore is given by $\hbar\omega_0(t)$, and the Rabi frequency Ω represents an interaction with an external light field of frequency ω_L [32]. The fluctuating protein matrix perturbs the intersection of the excited state of the *trans*-chromophore ($S_{1,\mathrm{trans}}$) and the electronic ground state of the *cis*-chromophore ($S_{0,\mathrm{cis}}$), causing a variation in the population of the *cis*-chromophores [26]. The slow modulation effects from the protein matrix are described by the stochastic transition matrices $\mathbb{M} = \{\overleftrightarrow{M}_1(t), \overleftrightarrow{M}_2(t), \overleftrightarrow{M}_3(t)\}$, corresponding to the photoactivation to the fluorescent on-state, the reversible switching to the off-state, and the irreversible conversion to the photobleached state of KFP1, respectively. The memory kernel $K(t)$ describes a photoblinking phenomenon of the chromophore due to a coupling to the fast fluctuating protein matrix.

B. Photon emission statistics of single-molecule fluorescent protein

The photon emission from an open quantum system can be calculated by decomposing the generating function of Eq. (1) into the dipole moment $U(t,s)$, the dipole current $V(t,s)$, the population inversion $W(t,s)$, and the total probability $Y(t,s)$ as detailed by Zheng *et al.* [30]. By converting $\mathcal{U}(t,s) = U(t,s)e^{\int_0^t d\tau\mathbb{M}(\tau)}$, $\mathcal{V}(t,s) = V(t,s)e^{\int_0^t d\tau\mathbb{M}(\tau)}$, $\mathcal{W}(t,s) = W(t,s)e^{\int_0^t d\tau\mathbb{M}(\tau)}$, and $\mathcal{Y}(t,s) = Y(t,s)e^{\int_0^t d\tau\mathbb{M}(\tau)}$, we derived the generalized optical Bloch equations with the aid of Budini′s prescription [29],

$$\dot{\mathcal{U}}(t,s) = -\frac{1}{2}[K_c * \mathcal{U}](t,s) + \mathbb{M}\mathcal{U}(t,s), \tag{2a}$$

$$\dot{\mathcal{V}}(\tau,s) = -\frac{1}{2}[K_c * \mathcal{V}](t,s) - \Omega\mathcal{W}(t,s) + \mathbb{M}\mathcal{V}(t,s), \tag{2b}$$

$$\dot{\mathcal{W}}(t,s) = \Omega\mathcal{V} - \frac{1+s}{2}[K * (\mathcal{W}+\mathcal{Y})](t,s) + \mathbb{M}\mathcal{W}(t,s), \tag{2c}$$

$$\dot{\mathcal{Y}}(t,s) = \frac{s-1}{2}[K * (\mathcal{W}+\mathcal{Y})](t,s) + \mathbb{M}\mathcal{Y}(t,s) \tag{2d}$$

for the open quantum system. Here $K_c(t) = K(t)\cos(\omega_L t)$, and "$*$" denotes a time-dependent convolution. Notice that the optical field oscillates much more rapidly than the memory kernel $K(t)$, thus the convolution operation of $\mathcal{U}(t,s)$ and $\mathcal{V}(t,s)$ with $K_c(t)$ can be reduced to a simple rate constant γ. We solved Eq. (2) in the Laplace domain u and derived

$$\bar{Y}(u,s) = \frac{(K+u)(u+\gamma/2)+\Omega^2}{2u(u+K)(u+\gamma/2)+2\,\Omega^2[u+(1-s)K/2]}. \tag{3}$$

The expectation value of the photon number can then be calculated with $\langle N\rangle(t) = 2\partial_s\mathcal{Y}(t,s)\,|_{s=1} = 2P_{\mathrm{on}}(t)\partial_s Y(t,s)\,|_{s=1}$. Here $P_{\mathrm{on}}(t)$ denotes the on-state probability density function

along the reactive coordinate Q_H. $P_{on}(t)$ and the other two probability density functions of the off-state (P_{off}) and the dark-state (P_{dark}) follow the reaction kinetics

$$P_{off} \underset{\overleftarrow{M}_2(t)}{\overset{\overleftarrow{M}_1(t)}{\rightleftharpoons}} P_{on} \overset{\overleftarrow{M}_3(t)}{\rightharpoonup} P_{dark}. \quad (4)$$

The reaction kinetics can then be described by

$$\begin{aligned} \partial_t P_{off}(t) &= -\overleftarrow{M}_1(t) P_{off}(t) + \overleftarrow{M}_2(t) P_{on}(t), \\ \partial_t P_{on}(t) &= \overleftarrow{M}_1(t) P_{off}(t) - [\overleftarrow{M}_2(t) + \overleftarrow{M}_3(t)] P_{on}(t), \\ \partial_t P_{dark}(t) &= \overleftarrow{M}_3(t) P_{on}(t) \end{aligned} \quad (5)$$

with the initial conditions $P_{off}(0) = 1$, $P_{on}(0) = 0$, $P_{dark}(0) = 0$, and $P_{off}(t) + P_{on}(t) + P_{dark}(t) = 1$.

To gain insight into the energy landscape evolution, we modeled the photoblinking dynamics with $K(u) = \gamma\{1 + [\beta(u+\phi)^{-1}]\}^{-1}$ [28], where β denotes the transition rate from the excited state $|b\rangle$ to the triplet state $|T\rangle$, and the transition rate of the reverse process is ϕ with a probability function $w_\phi(t)$ [29,33]. From Eq. (3), we derived the expectation value of photons emitted at time t as

$$\langle N \rangle (t) = \frac{\Omega^2 \gamma P_{on}(t) t}{\{\gamma^2 + 2\Omega^2[1 + \beta / w_\phi(t)]\}}. \quad (6)$$

III. METHODS

We installed a single-molecule optical apparatus to acquire the experimental data needed to test our formalization. The apparatus was equipped with a continuous-wave laser at 532 nm as the excitation light source and a 473-nm laser to quench KFP1 molecules. Both lasers were controlled with an acousto-optic tunable filter and circularly polarized to minimize the polarization-dependent effects. We focused the excitation light at the back focal plane of a 60× objective lens to epi-irradiate the sample. The fluorescent light emitted from the sample was collected by the same objective lens and detected with an electron-multiplying charge-coupled device.

The samples were prepared by suspending 1 nM KFP1 molecules in phosphate buffered saline containing 1% agarose gel and were fixed between two clean glass cover slips. After cooling the samples to below the softening temperature of the gel, we immobilized KFP1 molecules in the nanopores of the agarose gel matrix to keep all the KFP1 molecules as close to their native environment as possible. The methods of experiment and simulation are available online [34].

IV. RESULTS AND DISCUSSION

A. Light-emitting property of single-molecule KFP1

We irradiated the samples with the 532 nm laser and superposed the excitation beam with periodically pulsed light at 473 nm. Figure 2(a) presents a typical result of the experimental observation on an ensemble of KFP1 molecules. The fluorescent signal (shown by red squares) was periodically reduced to the level of the off-state by the pulsed 473 nm light, clearly revealing a photoswitching activity of the KFP1 molecules.

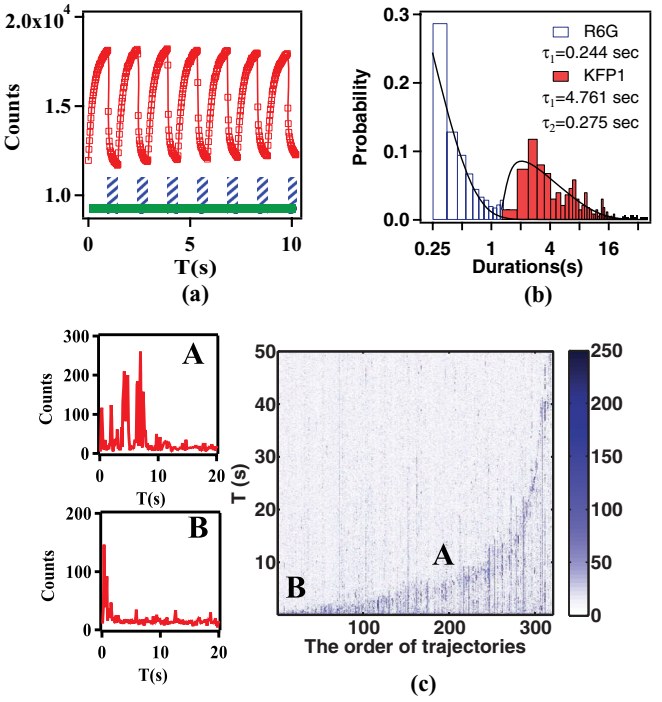

FIG. 2. (Color online) (a) Fluorescent signal at 630 nm (red open squares) from a film of KFP1 molecules embedded in agarose gel. The film was continuously irradiated by a 532 nm laser superposed with periodically pulsed light at 473 nm (the blue bars with the slash pattern). (b) Statistics of single-molecule photon emission from rhodamine 6G dyes (blue open bars) and from KFP1 molecules (red solid bars). (c) The measured fluorescent photon fluctuation traces from each single-molecule KFP1 are shown in the order of short to long light-emitting duration along the x axis.

For single-molecule measurements, we first irradiated a fresh sample with the 473-nm laser to convert the KFP1 molecules into the fluorescent off-state. Afterward, we recorded the traces of photon emission from each of the KFP1 molecules excited by the 532-nm laser. The single-molecule measurements reveal that 93% of the 345 KFP1 molecules are in the native states. The remaining 7% of the molecules behave like free fluorophores, presumably due to denaturation of KFP1. Figure 2(b) shows the survival probabilities of KFP1 and rhodamine 6G molecules continuously irradiated with the 532-nm laser. The statistics of the emitted photons from the KFP1 molecules (red solid bars) clearly differs from the free rhodamine 6G chromophores (blue open bars). The statistics of the photons emitted by the rhodamine 6G fits well to a single exponential decay function $P(t, \tau_1) = \tau_1 e^{-t/\tau_1}$ with a photobleaching lifetime of $\tau_1 = 0.244$ s. For KFP1, the probability function was found to be a convolution of two exponential functions as $P(t, \tau_1) \otimes P(t, \tau_2)$, with $\tau_1 = 4.761$ s denoting the photobleaching lifetime and $\tau_2 = 0.275$ s the lifetime of reversible kindling of KFP1.

In Fig. 2(c), we presented the measured photon traces of each KFP1 in the native states, arranged in order from short to long light-emitting duration. Two traces marked with A and B on the x axis are shown on the left side of the figure. The major

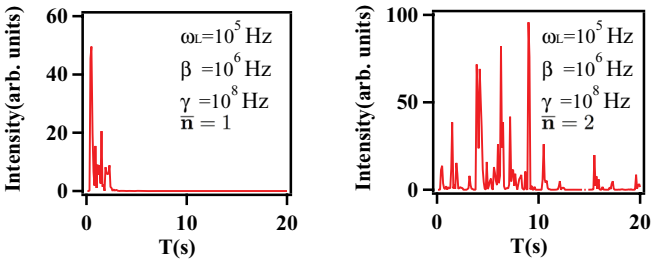

FIG. 3. (Color online) Calculated photon emission traces using $\Omega = 10^5$ Hz, $\beta = 10^6$ Hz, and $\gamma = 10^8$ Hz are shown in (a) with $\overline{n} = 1$ and (b) with $\overline{n} = 2$.

difference between the two photon traces originates from a difference in overcoming the barriers between two basins on the energy landscape, which is to be illustrated further in the following section.

B. Modeling the stochastic evolution on the energy landscape

Based on the principle of detailed balance, we assume the potential difference of the off-state and the on-state of KFP1 to be zero, which yields $\overleftrightarrow{M}_1 = \overleftrightarrow{M}_2$. The irreversible photobleaching converts the anionic chromophore to the dark state in the same *cis*-configuration. Thus, the stochastic transition $\overleftrightarrow{M}_3$ can be modeled with an exponentially distributed energy barrier. At each time step of Eq. (5), we invoked the Metropolis-Hastings algorithm [35] to sample the stochastic transition matrices $\mathbb{M}$, and we generated the probability density functions $P_{\rm on}(t)$. Equation (6) was then applied to unravel the single-molecule dynamics of KFP1.

To yield a clear physical picture of the stochastic transition matrices $\mathbb{M}$, we use a stochastic hopping model to facilitate our further discussion. A single hopping between two basins yields an exponential distribution with a characteristic energy parameter E_0. For N hopping steps, we shall obtain a gamma distribution $\Gamma(E;S,E_0)$ with a shape parameter S and a characteristic energy E_0. Our stochastic hopping picture yields a gamma distribution $\Gamma(E;\overline{n},E_0)$ with a shape parameter given by the mean number of traps. From a fluorescent signal trace measured on an ensemble of KFP1 molecules [36], we can determine the characteristic energy E_0 to be 0.19 eV [34]. Two photon emission traces calculated with Eq. (6) using $\Omega = 10^5$ Hz, $\beta = 10^6$ Hz, and $\gamma = 10^8$ Hz are shown in Fig. 3(a) with $\overline{n} = 1$ and in Fig. 3(b) with $\overline{n} = 2$.

The difference observed in Fig. 3 can be understood as follows: For a stochastic transition on an energy landscape, larger $\overline{n}$ implies stronger trapping at each site between two energy basins, making it more difficult for a KFP1 in the off-state to reach the on-state. Therefore, given a photobleaching rate, the dark-state probability is lower than that with smaller $\overline{n}$. This implies that the chromophore with larger $\overline{n}$ can survive longer under a constant irradiation and yields a longer duration of photon emission.

C. Dynamic regulation of photon emission by slow fluctuation of the protein matrix

Equation (6) also reveals a good log-linearity for the duration of photon emission as a function of the mean number

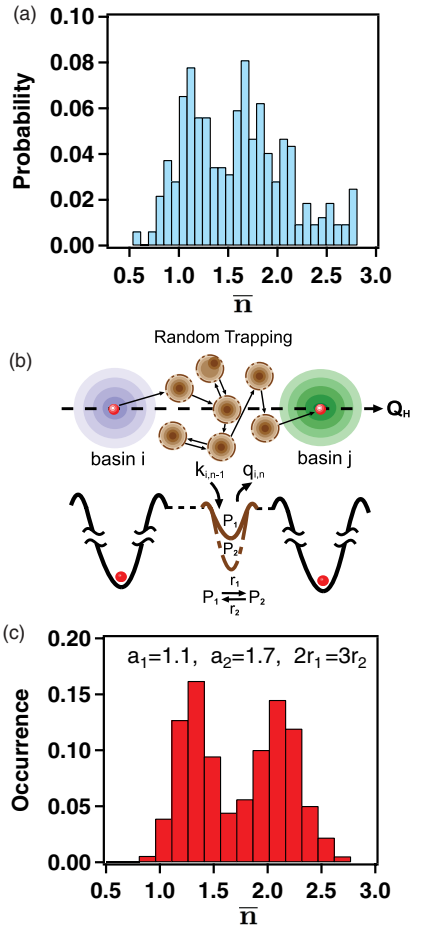

FIG. 4. (Color online) (a) A distribution of the mean number of traps was deduced from the KFP1 data set shown in Fig. 2(c). (b) A model of the stochastic hopping between two basins on the energy landscape of an active center along the reactive coordinate Q_H. (c) The calculated distribution of the mean number of traps with $a_1 = 1.1$, $a_2 = 1.7$, and $2r_1 = 3r_2$.

of traps [34]. We used this scaling to convert the measured fluorescent signal traces [shown in Fig. 2(c)] from the time domain to $\overline{n}$. We analyzed the data set and produced a histogram of $\overline{n}$. The distribution function reveals a bimodal profile as shown in Fig. 4(a), indicating that in KFP1 molecules the mean number of traps between two energy basins falls into two subsets.

To unravel the underlying mechanism of the observed bimodal profile, a stochastic hopping model was proposed [see Fig. 4(b)]. The occupation probability $P(n,t)$ at the nth intermediate site satisfies the chemical master equation $\partial_t P(n,t) = -q_n P(n,t) + k_{n-1} P(n-1,t)$. Here q_n denotes the escaping strength from the nth site and k_{n-1} is the trapping strength at the $(n-1)$th site. k_{n-1} and q_n follow Boltzmann's canonical distribution $k_{n-1}/q_n = e^{-(F_{n-1}-F_n)} = e^{-\Delta F_{n-1}}$ with a free energy difference ΔF_{n-1}. We split the free energy difference $\Delta F_{n-1} = \Delta\overline{E} - S_{n-1}$ into a mean energy difference $\Delta\overline{E}$ and an entropy term S_{n-1}. S_{n-1} reflects the freedom to choose the pathways, $S_{n-1} = \ln(\frac{P_{\rm trap}(n)}{P_{\rm escape}(n-1)})$. Based on the stochastic hopping model, the molecule at the nth site has

n different trapping pathways. But because the molecule can only escape from an occupied site, there is only one escaping pathway. Therefore, $S_{n-1} = \ln(\frac{1/n}{1}) = \ln(\frac{1}{n})$. The master equation yields $P(n) = \frac{e^{-\Delta\overline{E}}}{n} P(n-1)$ in a steady state. By invoking the reflective boundary condition $k_{-1} = q_0 = k_N = q_{N+1} = 0$ [37] and normalizing the probabilities to 1, the steady-state $P(n)$ becomes

$$P(n) = \frac{\frac{a^n}{n!}}{1 + \sum_{m=1}^{N} \frac{a^m}{m!}} \xrightarrow{N \gg 1} \frac{a^n e^{-a}}{n!}, \tag{7}$$

where $a = e^{-\Delta\overline{E}}$ is a dimensionless trapping strength, which is equal to $\overline{n}$. A hidden slowly fluctuating parameter is assumed to allow an interconversion between two groups of traps with trapping strength centering at a_1 and a_2, respectively. The forward (backward) conversion proceeds with a rate constant of r_1 (r_2), leading to an equilibrium constant of $K_{\rm eq} = r_1/r_2$. Including the interconversion process ($i : 1 \leftrightarrow 2$) into the master equation, we obtained

$$\begin{aligned} \partial_t P_1(n,t) &= -q_{1,n} P_1(n,t) + k_{1,n-1} P_1(n-1,t) \\ &\quad + r_2 P_2(n,t) - r_1 P_1(n,t), \\ \partial_t P_2(n,t) &= -q_{2,n} P_2(n,t) + k_{2,n-1} P_2(n-1,t) \\ &\quad - r_2 P_2(n,t) + r_1 P_1(n,t) \end{aligned} \tag{8}$$

in terms of the trapping strengths $k_{i,n-1}$ at the $(n-1)$th site and escaping strengths $q_{i,n}$ from the nth site. The stochastic hopping model yields $k_{i,n-1}/q_{i,n} = a_i/n$. Letting $r_1 = r_2 = 0$, Eq. (8) has a steady-state solution of $P_i(n) = a_i^n e^{-a_i}/n!$ ($i = 1$ or 2). Substituting the steady-state solution into Eq. (8) and assuming small r_1 and r_2 for a very slow interconversion process, we found that the steady-state solution of Eq. (8) satisfies $P_1(n)/P_2(n) = r_2/r_1$. The total occupation probability $P_t(n)$ is a weighted sum of $P_1(n)$ and $P_2(n)$, and by invoking the detailed balance principle $r_1 P_1(n) = r_2 P_2(n)$, we obtained

$$P_t(n) = \frac{r_2 P_1(n) + r_1 P_2(n)}{r_1 + r_2}. \tag{9}$$

The stochastic hopping dynamics exhibits a Γ distribution $\Gamma(E; P_t(n), E_0)$ with a shape parameter given by $P_t(n)$. By setting $a_1 = 1.1$, $a_2 = 1.7$, $2r_1 = 3r_2$, and the characteristic energy $E_0 = 0.19$ eV, we calculated a set of photon-number traces with $\Omega = 10^5$ Hz, $\beta = 10^6$ Hz, and $\gamma = 10^8$ Hz. The histogram of $\overline{n}$ assembled from the calculated traces is presented in Fig. 4(c). The simulation can reproduce the observed bimodal profile, implying that the model has captured the essential physics of dynamic regulation on the energy landscape of KFP1.

The ratio of r_1 and r_2, which specifies the equilibrium constant between the two groups of traps, yields a chemical potential difference $\Delta\mu = -k_B T \ln(K_{\rm eq}) = -10$ meV. The negative value implies that the environment tends to drive the single-molecule KFP1 away from its free-energy minimum. Note that for KFP1 in a thermally stable *cis*-chromophore, a hydrogen bonding can be formed between Glu215 and the N-H proton of the chromophore [26]. Thermal fluctuations of the protein matrix can perturb the degree of protonation in the hydrogen bonding and regulates the photon-emitting property of the chromophore. The chromophores of KFP1 molecules with a structural fit to the fluctuating protein matrix yield a distribution of trapping strength at $\overline{n} = 1.1$. These chromophores receive the benefit of minimum free energy and can take advantage of the thermal excitation to hop more rapidly on the energy landscape, while the other chromophores, which are slightly misfit to the fluctuating protein matrix, yield the peak at $\overline{n} = 1.7$ and hop between energy basins less efficiently.

Recently, Wright and co-workers [10] applied a mutation scheme to knock out the millisecond conformational fluctuations in the enzyme active site of *E. coli* dihydrofolate reductase. They observed a severe impairment on hydride transfer activity of the enzyme and revealed a direct link between the conformational fluctuations of a protein and the catalytic activity. Recently, Kruger and co-workers further showed that the intrinsic multifunctionality of plant light-harvesting complexes can be controlled by slow conformational fluctuations [38]. Our theoretical and experimental study verified that the slow fluctuations of a fluorescent protein can modulate its optical emission property by regulating the energy landscape evolution of the protein-embedded pigment.

V. CONCLUSIONS

In summary, we successfully developed a theoretical formalization for a rigorous description of photon emission from a single-molecule system comprising an active center and an environment relating to the protein matrix. We applied the formalization to analyze the statistics of photon emission from single-molecule photoactivated fluorescent KFP1 proteins. We found that dynamic transitions between conformational states of KFP1 are reflected in photon emission traces. The measured photon fluctuation traces from the protein-embedded active center fit well to a stochastic hopping picture with a different mean number of traps. We found a good log-linearity for the duration of photon emission as a function of the mean number of traps. Protein environment can induce slow fluctuations between conformations of a protein, which yields a bimodal regulation on the hopping strength and results in a guided stochastic evolution of the protein-embedded active center.

ACKNOWLEDGMENTS

Financial support from the National Science Council (NSC97-2112-M009-006-MY3) is gratefully acknowledged.

[1] E. Z. Eisenmesser, O. Millet, W. Labeikovsky, D. M. Korzhnev, M. Wolf-Watz, D. A. Bosco, J. J. Skalicky, L. E. Kay, and D. Kern, Nature (London) **438**, 117 (2005).

[2] K. A. Henzler-Wildman, V. Thai, M. Lei, M. Ott, M. Wolf-Watz, T. Fenn, E. Pozharski, M. A. Wilson, G. A. Petsko, M. Karplus, C. G. Hübner, and D. Kern, Nature (London) **450**, 838 (2007).

[3] K. Henzler-Wildman and D. Kern, Nature (London) **450**, 964 (2007).
[4] M. Diez, B. Zimmermann, M. Börsch, M. König, E. Schweinberger, S. Steigmiller, R. Reuter, S. Felekyan, V. Kudryavtsev, C. A. M. Seidel, and P. Gräber, Nat. Struct. Mol. Biol. **11**, 135 (2004).
[5] S. Uphoff, S. J. Holden, L. L. Reste, J. Periz, S. van de Linde, M. Heilemann, and A. N. Kapanidis, Nat. Methods **7**, 831 (2010).
[6] K. S. Karunatilaka, A. Solem, A. M. Pyle, and D. Rueda, Nature (London) **467**, 935 (2010).
[7] S. Yang, J. N. Onuchic, and H. Levine, J. Chem. Phys. **125**, 054910 (2006).
[8] R. B. Best and G. Hummer, Proc. Natl. Acad. Sci. (USA) **107**, 1088 (2010).
[9] D. E. Shaw, P. Maragakis, K. Lindorff-Larsen, S. Piana, R. O. Dror, M. P. Eastwood, J. A. Bank, J. M. Jumper, J. K. Salmon, Y. Shan, and W. Wriggers, Science **330**, 341 (2010).
[10] G. Bhabha, J. Lee, D. C. Ekiert, J. Gam, I. A. Wilson, H. J. Dyson, S. J. Benkovic, and P. E. Wright, Science **332**, 234 (2011).
[11] M. Samoilov, S. Plyasunov, and A. P. Arkin, Proc. Natl. Acad. Sci. (USA) **102**, 2310 (2005).
[12] C. A. Miller and D. A. Beard, Biophys. J. **95**, 2183 (2008).
[13] T. May, L. Eccleston, S. Herrmann, H. Hauser, J. Goncalves, and D. Wirth, PLoS ONE **3**, e2372 (2008).
[14] W. Yu, K. Chung, M. Cheon, M. Heo, K.-H. Han, S. Ham, and I. Chang, Proc. Natl. Acad. Sci. (USA) **105**, 2397 (2008).
[15] R. R. Cheng, T. Uzawa, K. W. Plaxco, and D. E. Makarov, J. Phys. Chem. B **113**, 14026 (2009).
[16] N. A. Sinitsyn, N. Hengartner, and I. Nemenman, Proc. Natl. Acad. Sci. (USA) **26**, 10546 (2009).
[17] H. S. Chung, J. M. Louis, and W. A. Eaton, Proc. Natl. Acad. Sci. (USA) **106**, 11837 (2009).
[18] T. Bornschlögl, G. Woehlke, and M. Rief, Proc. Natl. Acad. Sci. (USA) **106**, 6992 (2009).
[19] T. L. Religa, J. S. Markson, U. Mayor, S. M. V. Freund, and A. R. Fersht, Nature (London) **437**, 1053 (2005).
[20] D. J. Brockwell and S. E. Radford, Curr. Opin. Struct. Biol. **17**, 30 (2007).
[21] C. T. Friel, D. A. Smith, M. Vendruscolo, J. Gsponer, and S. E. Radford, Nat. Struct. Mol. Biol. **16**, 318 (2009).
[22] A. I. Bartlett and S. E. Radford, Nat. Struct. Mol. Biol. **16**, 582 (2009).
[23] K. A. Lukyanov, D. M. Chudakov, S. Lukyanov, and V. V. Verkhusha, Nat. Rev. Mol. Cell Bio. **6**, 885 (2005).
[24] B. Grigorenko, A. Savitskyb, I. Topolc, S. Burtc, and A. Nemukhin, Chem. Phys. Lett. **424**, 184 (2006).
[25] L. V. Schäfer, G. Groenhof, A. R. Klingen, G. M. Ullmann, M. Boggio-Pasqua, M. A. Robb, and H. Grubmüller, Angew. Chem. **119**, 536 (2007).
[26] L. V. Schäfer, G. Groenhof, M. Boggio-Pasqua, M. A. Robb, and H. Grubmüller, PLoS Comput. Biol. **4**, e1000034 (2008).
[27] W. Min, G. Luo, B. J. Cherayil, S. C. Kou, and X. S. Xie, Phys. Rev. Lett. **94**, 198302 (2005).
[28] A. A. Budini, Phys. Rev. E **72**, 056106 (2005).
[29] A. A. Budini, J. Chem. Phys. **126**, 054101 (2007).
[30] Y. Zheng and F. L. H. Brown, Phys. Rev. Lett. **90**, 238305 (2003).
[31] X.-Z. Li, B. Walker, and A. Michaelides, Proc. Natl. Acad. Sci. (USA) **108**, 6369 (2011).
[32] C. Cohen-Tannoudji, J. Dupont-Roc, and G. Grynberg, *Atom-Photon Interactions* (Wiley-Interscience, New York, 1992).
[33] A. A. Budini, Phys. Rev. A **69**, 042107 (2004).
[34] See Supplemental Material at http://link.aps.org/supplemental/10.1103/PhysRevE.86.021925 for experimental methods and for the detailed method of simulation.
[35] D. Gamerman, *Markov Chain Monte Carlo: Stochastic Simulation of Bayesian Inference* (Taylor & Francis, London, 1997).
[36] P. Didier, L. Guidoni, and F. Bardou, Phys. Rev. Lett. **95**, 090602 (2005).
[37] N. V. Kampen, *Stochastic Processes in Physics and Chemistry*, 3rd ed. (North-Holland Personal Library, Amsterdam, 2007).
[38] T. P. J. Krüger, E. Wientjes, R. Croce, and R. van Grondelle, Proc. Natl. Acad. Sci. (USA) **108**, 13516 (2011).